DOI: 10.13009/EUCASS2019-538

Theoretical and Experimental Study of Combustion Instability in Hybrid Rocket Motors

Artur Elias de Morais Bertoldi, Mohammed Bouziane**, Jungpyo Lee*, Carlos Alberto Gurgel Veras***, Patrick Hendrick**** and Domenico Simone**

**University of Brasília*

Faculty of Gama, AE Projeção A, 72444-240, Brasília, Brazil, artur.bertoldi@aerospace.unb.br

***Royal Military Academy*

Avenue de la Renaissance 30, 1000 Brussels, Belgium, mohammed.bouziane@dymasec.be

**University of Brasília*

Faculty of Gama, AE Projeção A, 72444-240, Brasília, Brazil, jungpyo_lee@aerospace.unb.br

****University of Brasília*

Mechanical Engineering Department, 70910-900, Brasília, Brazil, gurgel@unb.br

*****Université Libre de Bruxelles*

F.D. Roosevelt Avenue 50, 1050 Brussels, Belgium, patrick.hendrick@ulb.ac.be

**University of Brasília*

Faculty of Gama, AE Projeção A, 72444-240, Brasília, Brazil, domenico.simone@aerospace.unb.br

Abstract

This work describes a theoretical and experimental study of combustion instability in hybrid rocket motors. Results are highlighting that the parameter $\Delta p/\bar{p}_c$ (pressure drop between tank and chamber scaled by average chamber pressure) plays an important role in the oscillatory characteristics of the chamber pressure. By modifying the feed-system-coupled instability theory, a combustion time lag model has been developed; using this a new general analysis criterion is proposed. Results show good agreement with the experimental data and suggest that the combustion time delay of the liquid oxidizer is more important than the response time of solid fuel boundary layer.

1. Introduction

Hybrid rocket motors have been experiencing combustion instabilities problems in various projects at different motor scales. Studies on these phenomena suggest the existence of at least three major categories of hybrid combustion instabilities. One of these, due to the lag time associated with vaporization and combustion of liquid droplets, is similar to that in the liquid propellant motors but probably more complex, being the lag time affected by solid-liquid interface processes. A second family is characterized by an unstable combustion associated with periodic accumulation and breakoff of char layers or melted layers at the surface. The resulting instability is generally of low frequency (like "chuffing") and occurs during operation at low regression rates. In the third group the combustion instability mechanism is similar to that encountered in solid propellants. Here the acoustic admittance of the reacting turbulent boundary layers plays a key role, and the instability becomes more severe in presence of a pressure-sensitive regression rate [1].

Due to the lack of global theoretical models, many researches have been focused on explaining the instabilities connected with different specific operative modes of the motor. Special attention is given to the instabilities connected to the combustion at low frequencies. In this special case most of the experiments rely on gaseous oxidizers with sonic orifices, used to decouple the effects of the feed system from the motor combustion chamber. However, previous researches conducted at University of Brasilia (UnB) and at University of Brussels (ULB) using liquid oxidizers showed that the combustion chamber pressure oscillations were strongly influenced by injector design, pressure drop between tank and combustion chamber, combustion chamber length and size of the motor pre-chamber [2], [3], [4].

Thus, this work describes a theoretical and experimental study of combustion instability and the research aim is to develop a systematic approach devoted to characterize the combustion instability of hybrid motor during the conceptual design phase. An extension for the feed-system-coupled instability applied to hybrid motors using liquid oxidizers is formulated and a general instability analysis criterion is proposed. To investigate the instability related to the feed

DOI: 10.13009/EUCASS2019-538

system a series of tests have been carried out by UnB and ULB using liquid nitrous oxide as the oxidizer in a 1.0 kN hybrid motor.

2. Feed System Coupled Combustion Instability

The feed system coupled instability in liquid propellant rocket has been studied since the middle of the last century and some experimental and theoretical methodologies already exist to avoid or mitigates the problem. But in the hybrid propellant rockets this field is relatively new and actual [5], [6], [7]. Figure 1 shows a schematic of the atomization process in liquid engines. This process is analogous to hybrid propulsion based on the fact that hybrids have one of the propellants in liquid phase (usually the oxidizer) and the atomization process in this case play a major role over combustion instability.

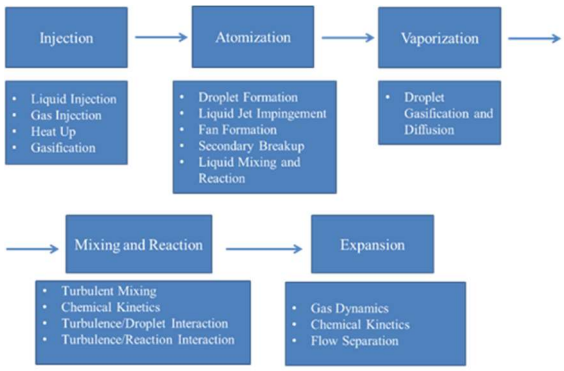

Figure 1: Atomization process in liquid rocket engines [8]

Figure 2 shows a simplified example of the main processes that happen inside a hybrid rocket combustion chamber. The thermal lag theory applied to the solid fuel already exist [9], [10], [11], but this theory does not take into account the injection of the liquid oxidizer, a key factor to design a commercial hybrid motor. The main objective of this study is to develop a first approach to understand the impact of the liquid injection over the hybrid combustion process and determine the main parameters for a stable operation of the motor.

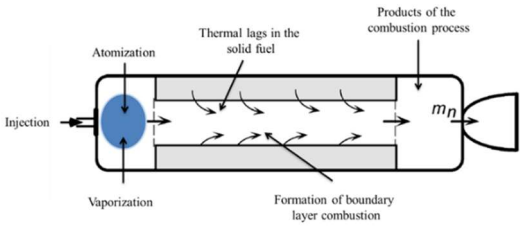

Figure 2: Chemical and physical process in hybrid rocket motors, simplified [3]

To stud the phenomena the main chamber was separated in two parts, the pre-chamber and fuel grain section. The influence of the post-chamber is not taken into account. Figure 3 presents the schematic of UnB SARA hybrid motor, where τ_1 is the combustion time delay of the liquid oxidizer and τ_2 is the combustion time delay of the solid fuel.

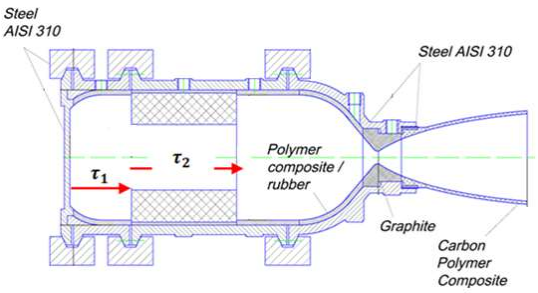

Figure 3: Representation of the characteristics time (τ_1 and τ_2) in UnB SARA hybrid motor [3]

DOI: 10.13009/EUCASS2019-538

In a time (t) is injected in the combustion chamber certain amount of liquid oxidizer $\dot{m}_{ox}(t)$. The processes of atomization, vaporization and mixing of the liquid oxidizer take a characteristic time, defined here as τ_1. Simultaneous, the fuel grain needs a characteristic time (τ_2) to react to the thermal process, diffusion and combustion. The mass equilibrium is given by Eq. (1), where $\dot{m}_n(t)$ is the amount of propellant leaving the nozzle at time *t*.

$$\frac{dm}{dt} = \dot{m}_{ox}(t) + \dot{m}_f(t) - \dot{m}_n(t) \tag{1}$$

The liquid oxidizer mass flow rate can be expressed as function of the oxidizer time delay $[\dot{m}_{ox,l}(t-\tau_1)]$, Eq. (2), and it represents that the oxidizer reacting with the fuel in time *t* was injected in time $t-\tau_1$. The gases flowing through the nozzle is expressed by Eq. (3). Where c_d is the coefficient of discharge, A_o the injector orifices area, ρ_{ox} the oxidizer density, p_T is the pressure in the oxidizer tanks, p_c the chamber pressure, c^*characteristic velocity and A_t is the nozzle throat area.

$$\dot{m}_{ox}(t) = \dot{m}_{ox,l}(t-\tau_1) = c_d A_o \sqrt{2\rho_{ox}(p_T - p_c)}\Big|_{(t-\tau_1)} \tag{2}$$

$$\dot{m}_n(t) = \frac{1}{c^*} p_c A_t \tag{3}$$

Fuel production is related with the regression rate $(\dot{r})$ and grain surface area (A_s), Eq. (4). The regression law can be written to the time $t-\tau_1$, Eq. (5); $\dot{m}_f$ is the fuel mass flow rate, p_f fuel density and A_s the surface area.

$$\dot{m}_f(t) = \rho_f A_s(t)\dot{r} = f(\dot{m}_{ox}(t-\tau_2)) \tag{4}$$

$$\dot{r}(t) = a G_{ox}^n|_{(t-\tau_2)} \tag{5}$$

Oxidizer mass flux is defined as $G_{ox}(t) = \dot{m}_{ox}/A_{port}$ [the port area, $A_{port} = \pi r^2$] and $\dot{m}_{ox}$ is the oxidizer mass flow rate. In Eq. (5) a and n are the regression rate coefficients. The solid fuel grain surface area is $A_s = 2\pi r L_f$ and L_f is the fuel length and r the fuel grain radius. Substituting it in Eq. (4) and regrouping the terms it is possible to express the fuel mass flow rate as:

$$\dot{m}_f(t) = a\,\rho_f A_s \left(\frac{\dot{m}_{ox,l}|_{(t-\tau_1)}}{A_{port}}\right)^n\Bigg|_{(t-\tau_2)} = a\,\rho_f \frac{A_s}{{A_{port}}^n} \dot{m}_{ox.l}^n|_{(t-\tau_1-\tau_2)} \tag{6}$$

The circular fuel grain length can be written in terms of the mixture ratio and others parameters in Eq. (7), where $K = 4^n p_f \pi^{1-n} a$ [12].

$$L_f = \frac{\dot{m}_{ox}^{1-n} \left(r/2\right)^{2n-1}}{K(O/F)} \quad (circular\ port) \tag{7}$$

Taking the ${A_s/A_{port}}^n$ and substituting Eq. (7), it gives:

$$\frac{A_s}{{A_{port}}^n} = \frac{\dot{m}_{ox}^{1-n}}{a\,\rho_f (O/F)} \cdot 2^{2-4n} \tag{8}$$

From mass flow rate definition $[\dot{m}_{ox}(t) = \dot{m}_{ox,l}(t-\tau_1)]$ and Eq. (8) is possible to re-write Eq. (6) as:

$$\dot{m}_f(t) = a\,\rho_f A_s \left(\frac{\dot{m}_{ox,l}|_{(t-\tau_1)}}{A_{port}}\right)^n\Bigg|_{(t-\tau_2)} = a\,\rho_f \left(\frac{2^{2-4n}}{a\,p_f(O/F)}\right)\left(\dot{m}_{ox,l}^{1-n} \cdot \dot{m}_{ox,l}^n\right)\Big|_{(t-\tau_1-\tau_2)} \tag{9}$$

DOI: 10.13009/EUCASS2019-538

Grouping the terms of Eq. (9), the fuel mass flow rate can be expressed by Eq. (10):

$$\dot{m}_f(t) = \left(\frac{2^{2-4n}}{(O/F)}\right)\left(\dot{m}_{ox,l}\right)\Big|_{(t-\tau_1-\tau_2)} \tag{10}$$

To most of hybrid motor applications the *n* coefficient might assumes values around 0.5 – 0.6. In this paper we used *n* as 0.5 for simplification purpose. It is a good approach for hybrids [3] and Eq. (10) can be written as bellow:

$$\dot{m}_f(t) = \frac{(\dot{m}_{ox,l})}{(O/F)}\Big|_{(t-\tau_1-\tau_2)} \tag{11}$$

Using Eq. (2) and Eq. (11) it is possible to re-write Eq. (1) as,

$$\frac{dm}{dt} = c_d A_o \sqrt{2\rho_{ox}(p_T - p_c)}\Big|_{(t-\tau_1)} + \frac{(\dot{m}_{ox,l})}{(O/F)}\Big|_{(t-\tau_1-\tau_2)} - \frac{1}{c^*} p_c A_t \tag{12}$$

Expressing in terms of pressure,

$$\frac{dp_c(t)}{dt} = \frac{RT_c}{V_c} c_d A_o \sqrt{2\rho_{ox}\Delta p}\Big|_{(t-\tau_1)} + \frac{RT_c}{V_c}\frac{c_d A_o \sqrt{2\rho_{ox}\Delta p}}{(O/F)}\Big|_{(t-\tau_1-\tau_2)} - \frac{RT_c}{V_c}\frac{1}{c^*} p_c A_t\Big|_t \tag{13}$$

Defining $\Delta p = p_T - p_c$ and introducing some pressure oscillation over the mean, $p_c = \bar{p}_c + p'$ and $L^* = V_c/A_t$ (motor characteristic length), Eq.(13) becomes:

$$\frac{dpc(t)}{dt} = \frac{\bar{p}_c}{\tau_r}\frac{1}{\xi}\left[1 - \frac{1}{2}\frac{p'}{(p_T - \bar{p}_c)}\right]_{(t-\tau_1)} + \frac{\bar{p}_c}{\tau_r}\frac{1}{\xi'}\left[1 - \frac{1}{2}\frac{p'}{(p_T - \bar{p}_c)}\right]_{(t-\tau_1-\tau_2)} - \frac{p_c}{\tau_r}\Big|_t \tag{14}$$

Where $\xi' = \xi \cdot (O/F)$ and $\xi = (O/F) + [1/(O/F)]$. It results in:

$$\frac{d\phi}{dt} + \frac{\phi}{\tau_r} = -\frac{\phi\beta}{\tau_r}\Big|_{(t-\tau_1)} - \frac{\phi\beta}{\tau_r}\Big|_{(t-\tau_1-\tau_2)} \tag{15}$$

This equation is similar to the liquid rocket propulsion case, with an additional term due the solid fuel. Solving it for the real and imaginary parts:

$$\alpha + \frac{1}{\tau_r} = -\frac{\beta}{\tau_r}\left\{e^{-\alpha\tau_1}\cos(\tau_1\omega) + e^{-\alpha(\tau_1+\tau_2)}\cos[(\tau_1+\tau_2)\omega]\right\} \tag{16}$$

$$\omega = \frac{\beta}{\tau_r}\left\{e^{-\alpha\tau_1}\sin(\tau_1\omega) + e^{-\alpha(\tau_1+\tau_2)}\sin[(\tau_1+\tau_2)\omega]\right\} \tag{17}$$

The trivial solution is α=0 (stability criteria) gives,

$$1 = -\beta\{\cos(\tau_1\omega) + \cos[(\tau_1+\tau_2)\omega]\} \tag{18}$$

$$\omega = \frac{\beta}{\tau_r}\{\sin(\tau_1\omega) + \sin[(\tau_1+\tau_2)\omega]\} \tag{19}$$

Taking the sinusoidal equation and using the periodic function properties it is possible to write the following expression :

$$\frac{\tau_r\omega}{\beta} = 2\sin\left[(\tau_1 + {}^{\tau_2}/_2)\omega\right]\cos\left[(-{}^{\tau_2}/_2)\omega\right] \tag{20}$$

DOI: 10.13009/EUCASS2019-538

Solving to $\frac{(\tau_1+{}^{\tau_2}/_2)}{\tau_r}$ we have,

$$\frac{1}{2\beta} = \frac{(\tau_1+{}^{\tau_2}/_2)}{\tau_r} \tag{21}$$

Where $\beta = \frac{1}{2(p_{inj}-\bar{p}_c)/\bar{p}_c}$; $\emptyset = \frac{p'}{\bar{p}_c}$.

Eq. (21) is one solution of Eq. (15) to the critical case of no-oscillation in the combustion chamber. Figure 4 presents the Eq. (21) graphic.

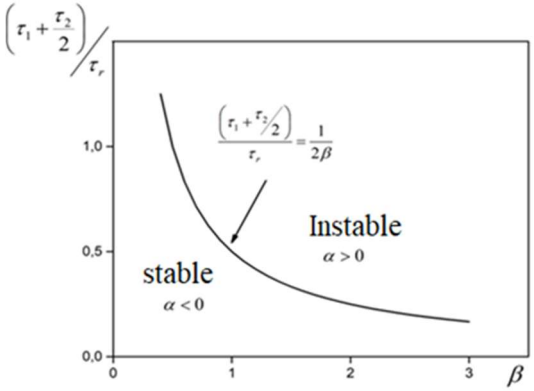

Figure 4: Stability limit for hybrid rocket motor

In the case of feed system instability for liquid rocket engines the limit $t_c \gg$ (combustion delay) leads to $\beta \to 1$, that implicates in Summerfield stability criteria $[\Delta p/\bar{p}_c > 1/2]$ for engine stable operation [3]. However, in the case of feed system instability for hybrids the Summerfield criteria is not applicable due the condition, $(\tau_1 + {}^{\tau_2}/_2) \gg; \beta \to 0$, which does not limit $\Delta p/\bar{p}_c$ values. Further, because the consumption of the fuel during the hybrid motor operation, the combustion chamber volume changes (increase) and this impact propellant residence time. It seems, in general aspects, that Eq. (21) and Figure 4 suggests that the instabilities in hybrid motors can be related with the liquid oxidizer feed system coupling to values higher than Summerfield criteria.

3. Experimental Setup

In this study is employed two hybrid rocket motors. The University Libre of Brussels (ULB) Hybrid Rocket Motor (ULBHRM) and the SARA motor from University of Brasília (UnB). The motors nominal parameters are presented in Table 1 and Figure 5 shows the SARA motor concept and Figure 6 the ULBHRM.

The CPL (Chemical Propulsion Laboratory) of the University of Brasilia (UnB) test bench is composed by the test stand, Data Acquisition System (DAQ) and the stand for personal. Figure 7 presents the graphical scheme of the sensor arrangements. Table 2 shows the type and main function of each sensor and gage used in CPL-UnB tests. Figure 8 introduces the schematic of the Aero-Thermo-Mechanics Department (ATM) of the University Libre of Brussels (ULB) test bench.

To study combustion instability of hybrid rocket motor using liquid oxidizer, some different types of injectors are applied. With SARA hybrid motor two types of injectors are used, in a total of three configurations. One is an axial injector with a single 10.25 mm diameter orifice (named AX10.25/1) and the other is showerhead injector (SH) in two configurations. SH:1-2/6-10 is composed by two radial symmetry set, 6 elements with 1mm diameter and 10 elements with 2 mm. And the second one (SH:2/16) has 16 orifices with 2 mm diameter [2], [3].

In the case of ULBHRM motor four different injectors were applied: (i) showerhead (SH); (ii) hollow cone (HC); pressure swirl atomizer (PSW) and vortex injector (VOR). Showerhead injector has two configurations, SH1 and SH2, with 11 and 21 elements, respectively, and each one has 1.4 orifice diameter. Hollow cone has 11 elements with 1.4 mm inclined 15º related with central-axis of motor. Pressure swirl atomizer also has two different configurations, PSW 1 and PSW2. PSW1 is composed by 6 elements, each one with 4 tangential holes, and an axial nozzle with 1.3 mm diameter. PSW2 has 9 individual injectors with a 1.5 mm diameter nozzle orifice. The VOR injectors are ordered in combination between axial and radial component, 45° each one, to distribute equally the flow towards the inner fuel grain surface [2], [3], [4]. Figure 9 shows SARA motor injector configuration and Figure 10 ULBHRM.

DOI: 10.13009/EUCASS2019-538

Table 1: Theoretical parameters of the ULBHRE

Parameter	SARA	ULBHRM
Thrust (nominal)	1 kN	1 kN
Operation time (*s*)	5 to 20	5 to 10
Chamber pressure	30 bar	20 to 30 bar
Propellant	N_2O/Paraffin	N_2O/Paraffin
O/F shift (nominal)	8	7.4
Expansion rate*	7.1	5.2

*Atmospheric nozzle

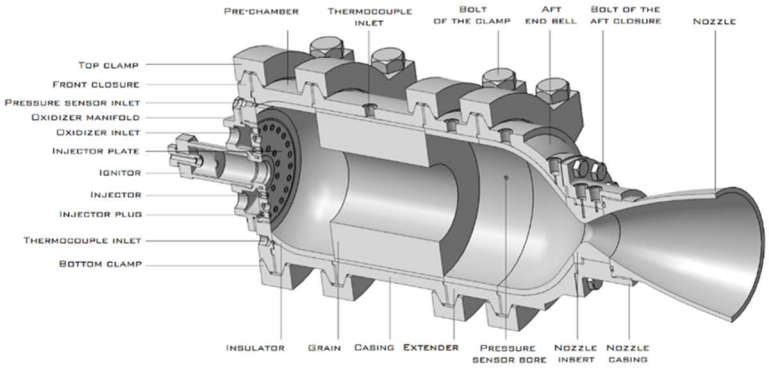

Figure 5: Design of SARA test motor [13]

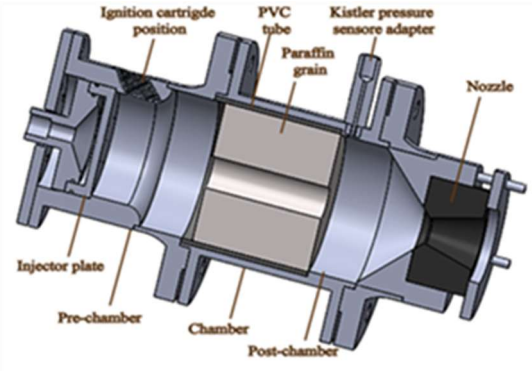

Figure 6: Design of ULBHRM test motor [14]

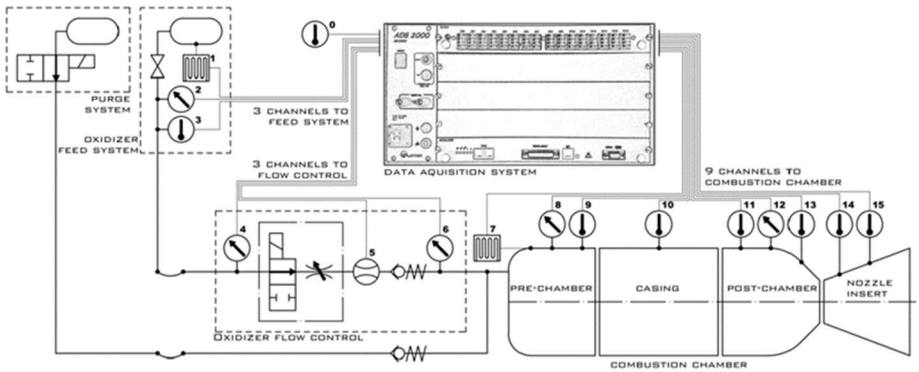

Figure 7: Arrangement of the sensor in SARA motor [13]

DOI: 10.13009/EUCASS2019-538

Table 2: Main sensors and purposes of the measurement [13]

Sensor/gage name	Position	Parameter to measure	Purpose
Thermocouple type K	0	Ambient temperature	Reference point for temperature distribution
	3	Oxidizer temperature	Control of oxidizer state
	9	Pre-chamber temperature	Control of thermal conduction in front insulator
	10	Grain temperature	Control of thermal conduction in grain
Thermocouple type N	11	Insulator temperature	Control of thermal conduction in aft insulator
	13-15	Aft closure temperature	Control of temperature in aft end bell and Nozzle
Load cell	1	Weight of the oxidizer tank	Monitoring of oxidizer flow rate
	7	Thrust of the motor	Study of motor performance
Pressure transducer	2	Pressure in oxidizer tank	Control of oxidizer state
	4 6	Pressure in oxidizer pipeline	Pressure drop control in valve
	12	Pressure in post-chamber	
Piezoelectric pressure sensor	8	Pressure in pre-chamber	Pressure control in motor

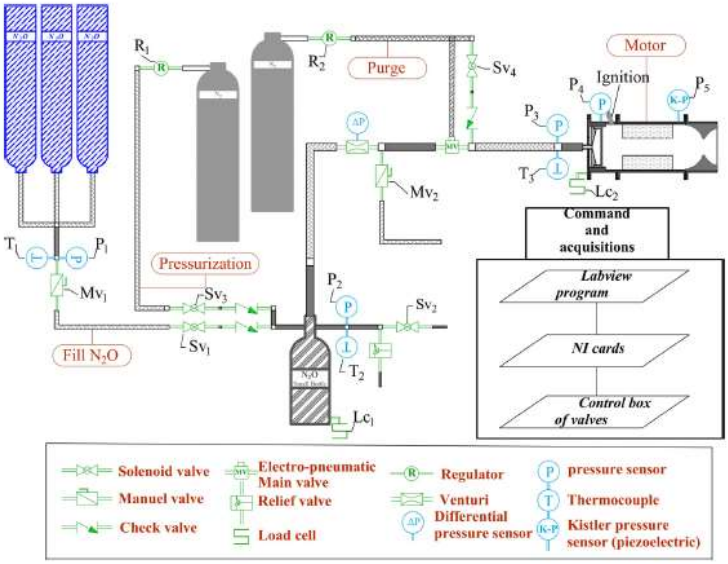

Figure 8: Schematic of ULBHRM test bench [14]

During the test phase of both engines it was observed pressure oscillations in the combustion chamber signal. In some test the oscillation amplitude was about 20% over the pressure chamber average value. Hence, an experimental study was performed to identify the major parameter that affects the combustion instability in hybrid motors.
In this work, the main combustion instability is related with the liquid oxidizer injection. Thus, the TCG-coupled theory [11] is not completely valid because it was developed for system with decouples the effects of the feed system over the motor performance by the means of gaseous oxidizer passing throughout a chocking orifice. Once that SARA and ULBHRM are designed to use liquid oxidizer the effects of the feed system coupled instabilities cannot be neglected.

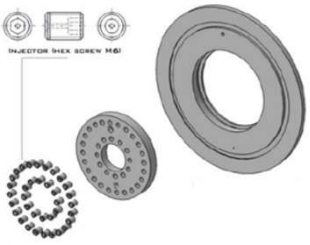

Figure 9: Modular injection system – configuration for SARA motor [13]

DOI: 10.13009/EUCASS2019-538

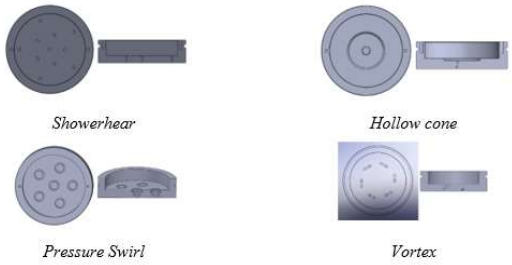

Figure 10: Configuration for ULBHRM motor [4]

4. Results

4.1 Fire test results

A series of tests were carried out with both motors. Table 3 gives the conditions for the tests with the SARA motor and Table 4 for the ULBHRM. The main parameters presented in the tables are the injector configuration, the pre-chamber length (L_{pc}), average chamber pressure ($\bar{p}_c$), oxidizer mass flow rate ($\dot{m}_{ox}$) and *O/F* ratio. For both motors tests the fuel initial port diameter and length was keep constant.

Table 3: Sara motor test conditions

Test	Injector	L_{pc} (mm)	$\bar{p}_c$ (bar)	$\dot{m}_{ox}$ (kg/s)	*O/F*
1	SH:1-2/6-10	56.6	25.2	0.211	2.8
2	SH:1-2/6-10	157.6	39.0	0.396	5.4
3	SH:1-2/6-10	56.6	36.5	0.339	5.1
4	SH:1-2/6-10	56.6	42.4	0.379	5.1
5	SH:1-2/6-10	56.6	40.7	0.432	5.5
6	SH:1-2/6-10	56.6	34.2	0.385	4.5
7	SH:1-2/6-10	56.6	41.0	0.317	3.0
8	SH:1-2/6-10	56.6	38.5	0.350	3.1
9	SH:1-2/6-10	56.6	44.9	0.317	2.8
10	SH:1-2/6-10	56.6	28.3	0.383	3.5
11	SH:1-2/6-10	56.6	35.5	0.350	4.2
12	AX:10.25/1	56.6	20.0	0.364	4.2
13	SH:2/16	56.6	42.0	0.559	6.5
14	AX:10.25/1	177.6	34.3	0.350	3.8
15	AX:10.25/1	76.6	36.2	0.260	4.3

Table 4: ULBHRE motor test conditions

Test	Injector	L_{pc} (mm)	$\bar{p}_c$ (bar)	$\dot{m}_{ox}$ (kg/s)	*O/F*
16	HC	102.5	19.8	0.413	2.4
17	HC	102.5	19.0	0.412	2.5
18	HC	102.5	18.5	0.410	2.4
19	HC	102.5	19.6	0.432	2.5
20	HC	102.5	19.3	0.427	2.6
21	PSW2	102.5	18.1	0.484	5.1
22	PSW2	102.5	20.8	0.544	5.4
23	SH1	102.5	17.7	0.405	3.5
24	SH1	102.5	16.5	0.380	2.5
25	SH1	102.5	16.8	0.390	2.8
26	SH2	102.5	24.0	0.540	3.8
27	SH2	102.5	22.7	0.576	3.8
28	SH2	102.5	23.5	0.552	3.7
29	SH2	102.5	25.3	0.646	4.1
30	SH2	102.5	29.9	0.608	3.8
31	SH2	102.5	23.3	0.538	3.5
32	SH2	102.5	27.4	0.621	3.9
33	VOR	102.5	26.2	0.531	3.3
34	VOR	102.5	26.2	0.544	3.5

To study the pressure oscillations in the combustion chamber it was used a kistler piezoelectric sensor type 6052CS31 to the CPL/UnB test and type 6061BS32 for ATM/ULB tests. The sample rate for UnB test was 5000 Hz and for ULB 8192 Hz. The FFT (Fast Fourier Transform) and STFT (Short-Time Fourier Transform) analysis were done by the use of the software Matlab. The others pressure in the system, nitrous oxide fed tank pressure (commercial cylinders), and nitrous oxide motor tank pressure, feed system pressure and combustion chamber pressure (backup sensor) were obtained with piezoresistive diaphragm type sensors.

DOI: 10.13009/EUCASS2019-538

The Figure 11 shows the average pressure in the motor systems (oxidize tank, feed system and combustion chamber) and Figure 12 chamber pressure oscillation for test number 15. The Figures 13 and 14 gives the same information for test number 26.

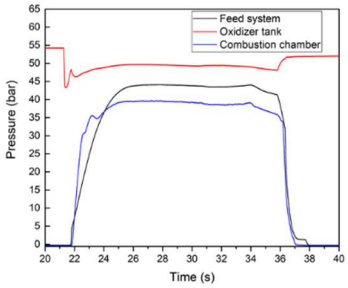

Figure 11: Main pressure signal in the systems for test #15

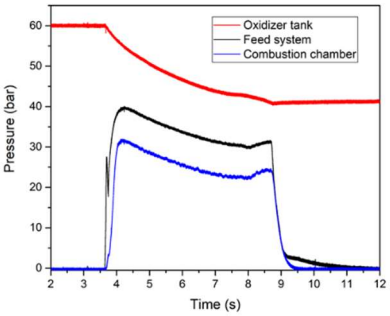

Figure 13: Main pressure signal in the systems for test #26

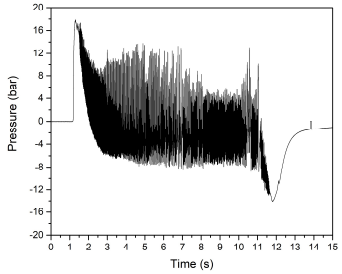

Figure 12: Combustion chamber pressure oscillations for test #15

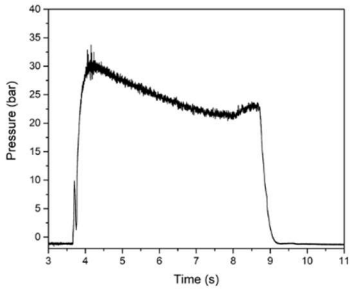

Figure 14: Combustion chamber pressure oscillations for test #26

By the analysis of the chamber pressure signal it is possible to note large amplitude of oscillation in the combustion chamber trace. For design and operation of the motor, it is necessary identify the main parameters that affects the combustion instability in order to try to predict the phenomena.

4.2 Implications of the combustion time lag theory for hybrid motors

The present study considers two lab-scale 1kN hybrid rockets using liquid nitrous oxide as oxidizer. During the test running it was observed feed-system coupled combustion instability, Figure 12 and Figure 14. In this cases, various physical quantities change in bulk mode when unstable combustion occurs in a hybrid combustion chamber. Here, we analyze the impact of the combustion time delay of the liquid oxidizer (τ_1) and combustion time delay of the solid fuel (τ_2). In Eq. (21), the variables β, τ_1, τ_2, τ_r are obteined from the motor tests data and geometry. The oxidizer characteristic time (τ_1) is calculated using the pre-chamber length (L_{pc}) and effective axial velocity in the pre-chamber ($\bar{u}_{x,ox}$).

$$\tau_1 = {L_{pc}}/{\bar{u}_{x,ox}} \tag{22}$$

And,

$$\bar{u}_{x,ox} = \frac{u_{inj}+u_{port}}{2} \tag{23}$$

Where $\bar{u}_{x,ox}$ is taken as an average value between the oxidizer velocity in the injector plate (u_{inj}) and velocity at the combustion port (u_{port}) entrance, which is expressed by the following equations:

$$u_{inj} = \frac{\dot{m}_{ox}}{\rho_{ox} A_o} \tag{24}$$

DOI: 10.13009/EUCASS2019-538

$$u_{port} = \frac{\dot{m}_{ox}}{\rho_{ox,port} A_{port}} \quad \textbf{(25)}$$

In Eq.(24) and Eq.(25) $\dot{m}_{ox}$ is the oxidizer mass flow rate, obtained experimentally, $\rho_{ox,\,inj}$ is the oxidizer density in the injector plate, $\rho_{ox,\,port}$ the density of the oxidizer entering in the fuel combustion port (assumed gaseous), A_o is the effective injector area and A_{port} is the combustion port.
To obtain τ_1 is necessary to estimates the liquid oxidizer density ($\rho_{ox,\,inj}$). In some cases, the assumption that oxidizer is completely liquid in the injector plate is a good approach. However, in hybrid rockets motors using nitrous oxide we have a multi-flow patter. Figure 15 shows a test with showerhead injector, during the characterization in cold test conditions, using water and Figure 16 presents the same injector test with nitrous oxide. All the injectors were characterized in the ULB – ATM Department. More information about the injectors and its characteristics can be found in reference [15].

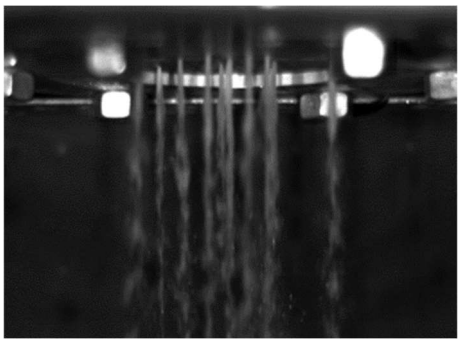

Figure 15: Showerhead injector characterization with water [14]

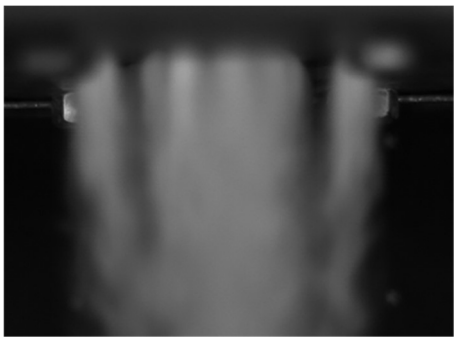

Figure 16: Showerhead injector characterization with N_2O [14]

As can be observed in Figure 16 and reference [15] the nitrous oxide becomes a mixing between gas and liquid even in the closer part of injector plate. For this reason, it was done a theoretical study [3] and we assumed 50% Liquid/Gas N_2O percentage. The others parameters can be found by experimental data analysis. Combustion time delay of the solid fuel (τ_2) where calculated taking into consideration TCG-Coupled Instability [11].
Table 5 summarizes the experimental results, the Fast Fourier Transform (FFT) over the entire signal, initial frequency (f), the first longitudinal acoustic mode (f_{1L}), (τ_1) and (τ_2). The pre-chamber length for each test can be found in tables 3 and 4. The tests from 1 to 15 were done with the SARA motor, therefore the test from 16 to 34 were carried out with ULBHRM.
Using table 3 and table 4 conditions associated with the results (table 5) it is possible use experimental data to apply the instability criteria derivate in Eq. (21), Figure 17. The injector identification is: AX – axial (single orifice), SH – shower head, HC – hollow cone, PSW – pressure-swirl injector and VOR – vortex injector.
By the analysis of the graph (Figure 17) and Eq. (21) results (Figure 4), it is possible to conclude that the preliminary calculation for the feed system coupled instability has good agreement with the experimental data for two different hybrid rocket motors tested in different universities.

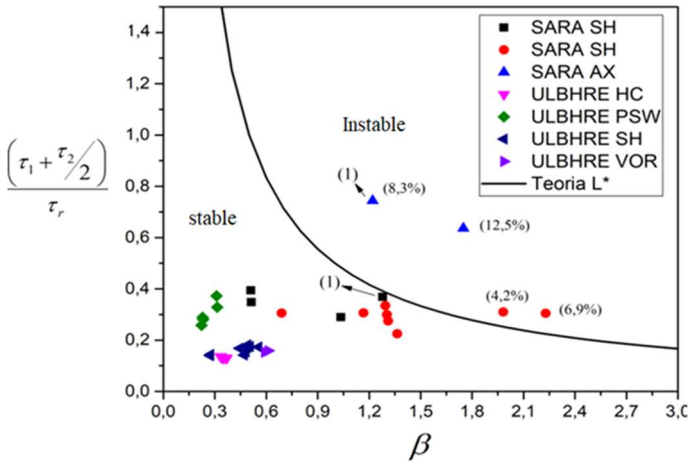

Figure 17: Stability criteria relating Eq.(21) and experimental results

DOI: 10.13009/EUCASS2019-538

Table 5: Frequency analysis

Test	*FFT* (Hz)	*f* (Hz) (initial)	f_{1L} (Hz)	τ_1 (ms)	τ_2 (ms)
1	9.6	44.5	1523.2	7.5	6.1
2	10.8	78.5	1184.2	11.9	4.3
3	83.5	122.3	1663.8	4.9	4.7
4	70.1	90.7	1666.8	4.5	4.9
5	93.1	119.9	1667.2	3.9	4.2
6	75.5	123.5	1636.6	4.3	4.4
7	106.1	140.5	1523.9	5.4	6.8
8	99.5	135.7	1532.0	4.8	5.6
9	101.9	133.2	1508.9	4.5	6.5
10	98.4	143.0	1585.9	4.2	3.6
11	94.3	141.8	1640.9	4.8	4.9
12	80.4	84.6	1645.0	19.8	3.4
13	125.1	127.2	1656.1	3.0	3.3
14	33.8	40.8	1085.1	16.4	6.3
15	38.7	53.0	1521.0	28.3	4.8
16	7.6	43.2	1199.4	3.8	2.7
17	8.2	43.0	1202.3	3.8	2.7
18	7.2	42.0	1199.3	3.8	2.6
19	7.2	44.5	1212.0	3.6	2.6
20	7.1	45.7	1204.8	3.7	2.6
21	14.2	38.6	1311.7	10.0	1.9
22	15.1	30.5	1312.9	8.9	1.9
23	7.8	39.6	1257.9	3.9	2.4
24	6.7	30.5	1203.2	4.0	2.5
25	30.5	31.7	1209.4	3.9	2.5
26	6.4	31.7	1277.8	5.1	2.4
27	7.4	35.3	1278.0	4.8	2.1
28	7.1	44.5	1272.2	5.0	2.3
29	7.0	34.1	1292.4	4.3	2.1
30	6.5	39.6	1278.9	4.4	2.6
31	6.5	34.1	1259.5	5.0	2.4
32	10.0	37.8	1284.4	4.4	2.3
33	8.0	35.6	1242.2	5.1	2.8
34	6.1	57.2	1258.5	5.1	2.7

4.3 Frequency analysis

To study the influence of τ_1 and τ_2 over the pressure oscillations in the combustion chamber a frequency analysis were carried out. For these tests the FFT analysis was performed over the entire chamber pressure signal and also for the initial values. Once that hybrid motors have a solid fuel being consumed in time, the fuel combustion port changes its dimensions, as consequence, the frequencies in the combustion chamber are not constant.

Figure 18 shows the result for test #1. In this test the FFT over the entire signal and the initial frequency are 9.6 Hz and 44.5 Hz, respectively. The oscillation amplitude over the average chamber pressure [$(\Delta p/\bar{p}_c)$%] is 0.7%. It represents a stable motor operation. Figure 19 presents the 2-D spectrogram and Figure 20 the real-time estimation of spectral density to the same test.

Figure 21 shows the result for test #4. In this test the FFT over the entire signal and the initial frequency are 70.1 Hz and 90.7 Hz, respectively. The oscillation amplitude over the average chamber pressure is 6.9%. It represents an instable motor operation. Figure 22 presents the 2-D spectrogram and Figure 23 the real-time estimation of spectral density.

Figure 24 shows the result for test #15. In this test the FFT over the entire signal and the initial frequency are 38.7 Hz and 53.0 Hz, respectively. The oscillation amplitude over the average chamber pressure was 12.5%. It represents an instable motor operation. Figure 25 presents the 2-D spectrogram and Figure 26 the real-time estimation of spectral density.

By the analysis of tests results, it is possible to affirm that for instable tests the frequency of spectral density over the complete signal decrease in time, as Figure 23 and Figure 26 illustrate. In the other hand, for stable tests do not exist any dominate frequency (in terms of amplitude) and this behaviour is exemplified by Figure 20. This comportment is the same for all 34 tests carried out in this research.

DOI: 10.13009/EUCASS2019-538

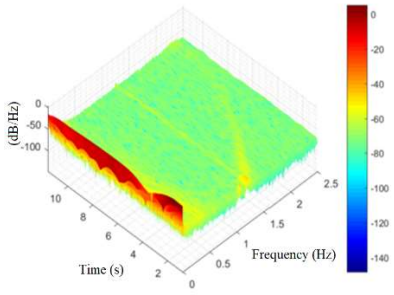

Figure 18: 3-D spectrogram for test #1

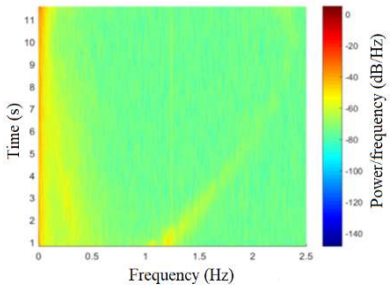

Figure 19: 2-D spectrogram for test #1

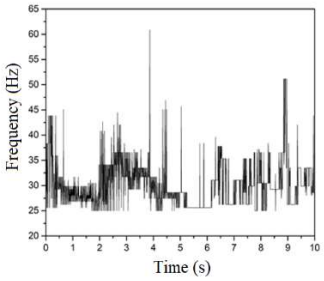

Figure 20: Real-time estimation of spectral density for test #1

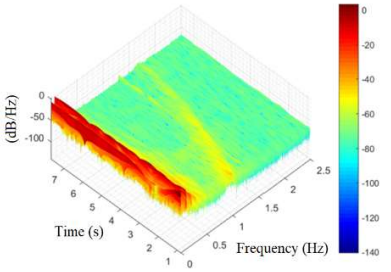

Figure 21: 3-D spectrogram for test #4

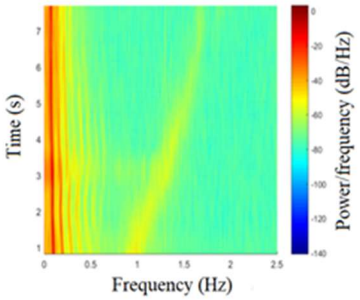

Figure 22: 2-D spectrogram for test #4

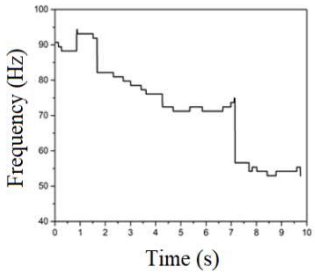

Figure 23: Real-time estimation of spectral density for test #4

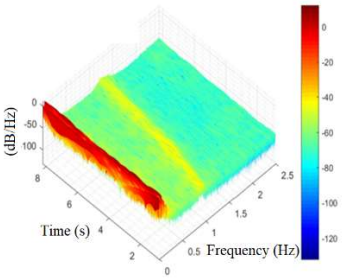

Figure 24: 3-D spectrogram for test #15

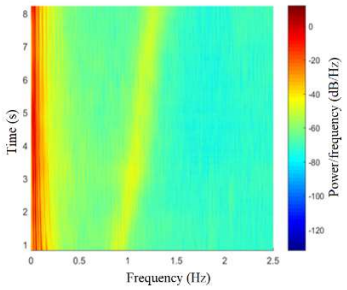

Figure 25: 2-D spectrogram for test #15

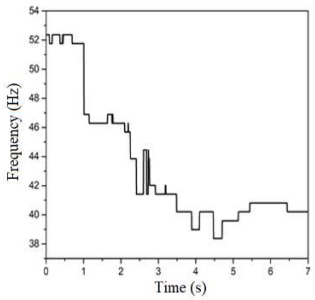

Figure 26: Real-time estimation of spectral density for test #15

DOI: 10.13009/EUCASS2019-538

Using data presented in Table 5 it is possible to plot the first frequency in function of τ_1 (Figure 27) and τ_2 (Figure 28). Figure 27 suggest a dependency between the first frequencies and τ_1 while in Figure 28 the relation among the first frequencies and τ_2 seems to be random.

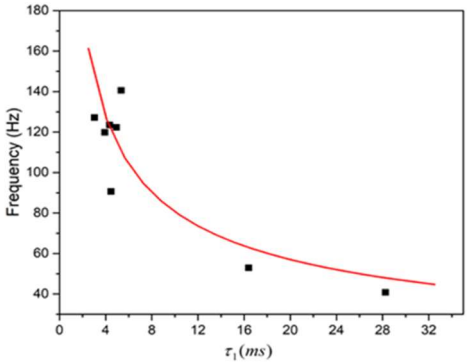

Figure 27: First chamber frequency in function of τ_1

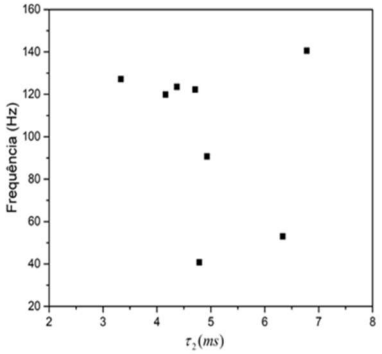

Figure 28: First chamber frequency in function of τ_2.

By the graph of Figure 27 it is possible to suggest a general equation to estimates the first non-acoustic chamber pressure frequency in function of the oxidizer characteristic time (τ_1). In Eq.(26) k' is a constant that needs to be determined empirically.

$$f = k' \frac{1}{\sqrt{\tau_1}} \quad \textbf{(26)}$$

4.4 Impact of the motor pre-chamber and oxidizer pressure drop over the combustion instability

Table 6 (page 14) presents the relation between the injectors, pressure chamber, pressure drop in the injector plate (Δp) and the pressure oscillation amplitude over the average value of the chamber pressure ($\Delta\%$). Results show that just changing the injector type it is possible to reduce chamber pressure amplitude oscillations from 12.5% (test #15) to less than 5% (test #3) to a closer $\Delta p/\bar{p}_c$ ratio.
The data analysis show that the influence of $\Delta p/\bar{p}_c$ is more important than the injector type and the pre-chamber length also has an impact over the stable behaviour, Table 7. In this way, the trade-off between the $\Delta p/\bar{p}_c$ and the pre-chamber length is important in order to control the pressure oscillations in the combustion chamber and at the same time keep the mass budget requirements.

Table 7: Pre-chamber influence over the pressure oscillations

Test	Injector Configuration	L_{pc} (mm)	$\Delta p/\bar{p}_c$	$\Delta p/\bar{p}_c$ (%)
1	SH:1-2/6-10	56.6	0.98	0.7
2	SH:1-2/6-10	157.6	0.39	0.3
3	SH:1-2/6-10	56.6	0.39	3.6
7	SH:1-2/6-10	56.6	0.38	3.6
9	SH:1-2/6-10	56.6	0.37	4.1
14	AX:10.25/1	177.6	0.41	8.3
15	AX:10.25/1	76.6	0.29	12.5

DOI: 10.13009/EUCASS2019-538

Table 6: Experimental data for motor tests;
$\Delta(\%)$ is the pressure oscillation amplitude $[(\Delta p/\bar{p}_c)\%]$

Test	Injector Configuration	p_c (bar)	Δp (bar)	Δ (%)
1	SH:1-2/6-10	25.2	24.7	0.7
2	SH:1-2/6-10	39.0	15.2	0.3
3	SH:1-2/6-10	36.5	14.1	3.6
4	SH:1-2/6-10	42.4	9.5	6.9
5	SH:1-2/6-10	40.7	10.3	4.2
6	SH:1-2/6-10	34.2	14.6	3.7
7	SH:1-2/6-10	41.0	15.6	3.6
8	SH:1-2/6-10	38.5	18.6	0.4
9	SH:1-2/6-10	44.9	16.5	4.1
10	SH:1-2/6-10	28.3	27.6	0.2
11	SH:1-2/6-10	35.5	25.7	1.7
12	AX:10.25/1	20.0	29.3	20.0
13	SH:2/16	42.0	16.1	5.1
14	AX:10.25/1	34.3	14.1	8.3
15	AX:10.25/1	36.2	10.4	12.5
16	HC	19.8	26.8	1.2
17	HC	19.0	28.1	1.7
18	HC	18.5	27.7	0.9
19	HC	19.6	26.7	1.1
20	HC	19.3	27.5	1.5
21	PSW2	18.1	29.2	1.5
22	PSW2	20.8	33.1	3.7
23	SH1	17.7	27.2	0.7
24	SH1	16.5	30.0	1.2
25	SH1	16.8	30.7	1.5
26	SH2	24.0	21.6	1.2
27	SH2	22.7	23.1	1.2
28	SH2	23.5	23.2	1.2
29	SH2	25.3	28.4	1.2
30	SH2	29.9	31.8	1.1
31	SH2	23.3	23.7	2.6
32	SH2	27.4	28.4	4.7
33	VOR	26.2	22.1	3.1
34	VOR	26.2	21.4	4.5

5. Conclusions

In this work the effects of the feed system on the chamber pressure have been investigated, and results show that the instability behaviour of the system are different from the TC-coupled instability, which is one of the system instabilities for hybrid rockets and caused by the fuel boundary layer response time. When a liquid oxidizer is used, the main frequencies of pressure oscillations are strongly influenced by the residence time in pre-chamber and by the flow characteristics; in some specific conditions, feed system instabilities can occur.

Analysing the variables related to liquid oxidizer (that influences the oscillatory characteristics of the chamber pressure) it is possible to observe that the parameter $\Delta p/\bar{p}_c$ plays an important role in the instability comportment. When $\Delta p/\bar{p}_c$ is higher than 0.7, the combustion chamber pressure oscillations are lower than 5% of the pressure chamber average values. In addition, it is evident that the pre-chamber configuration has an important influence on the oscillatory behaviour. In tests with long pre-chambers the stable condition is obtained for values of $\Delta p/\bar{p}_c$ even lower than 0.5. However, a long pre-chamber length penalizes the rocket motor weight, and should be considered after a trade-off analysis.

From the analysis of Eq. (21) and experimental data we can suggest that the instabilities in hybrid motors can be related with the liquid oxidizer feed system coupling, for values of $\Delta p/\bar{p}_c$ higher than 0.5 (Summerfield criteria for liquid rocket engines). In this case, Eq. (21) can be used as tool for preliminary analysis of combustion instability.

DOI: 10.13009/EUCASS2019-538

It can be also confirmed that the combustion time delay of the liquid oxidizer (τ_1) is more important than the response time of solid fuel boundary layer (τ_2). Based on experimental data and on the feed system coupled instability model, Eq. (26) can be used to estimates the fundamental frequency of the feed system coupled instability as a function of the oxidizer characteristic time (τ_1).

Acknowledgements

Prof. A. E. M. Bertoldi would like to express his thanks to the Brazilian Space Agency (AEB) and Brazilian National Council for Scientific and Technological Development (CNPq) and the authors thanks the technicians of Aero-Thermo-Mechanics at ULB and chemical department at Royal Military Academy of Belgium for their helps.

References

[1] National Aeronautics and Space Administration-NASA, Langley Research Center (USA). Investigation of Combustion Instability in Hybrid Rockets, (1969). Report. NASA CR-66812. SRI, California, 34p.

[2] Bertoldi, A.E.M., Bouziane, M., Veras, C.A.G., Lee, J., Costa, M.V.C. (2018). Experimental Investigation of the Feed System Instabilities in Hybrid Rocket Motors. In : 69th International Astronautical Congress (IAC), Bremen, Germany.

[3] Bertoldi, A.E.M. (2018). Estudo de Instabilidade de Combustão em Motor Foguete a Propelente Híbrido. PhD thesis, University of Brasília, Mechanical Engineering Department, in Portuguese.

[4] Bouziane, M., Bertoldi, A.E.M., Milova, P., Hendrick, P., Lefebvre. (2019). Performance Comparison of Oxidizer Injectors in a 1-kN Paraffin-Fueled Hybrid Rocket Motor. Aerospace Science and Technology, vol. 89 (2019), 392 – 406p.

[5] Story, G., Zoladz, T., Arves, J., Kearney, D., Abel, T., Park, T. (2003). Hybrid Propulsion Demonstration Program 250K Hybrid Motor. In: 39th AAAI/ASME/SAE/ASEE Joint Propulsion conference and Exhibit, Huntsville, AL, USA.

[6] Morita, T., Kitagawa, K., Yuasa, S. Yamaguchi, S., Shimada, T. (2012). Low-Frequency Combustion Instability Induced by the Combustion Time Lag of Liquid Oxidizer in Hybrid Rocket Motors. Transactions of the Japan Society for Aeronautical and Space Sciences (JSASS), Aerospace Technology Japan, vol. 10, 37- 41p.

[7] Waxman, B., Zimmerman, J.E., Cantwell, B. (2014). Effects of Injector Design on Combustion Stability in Hybrid Rockets Using Self-Pressurizing Oxidizers. In: 50th AIAA/ASME/SAE/ASEE Joint Propulsion Conference. Cleveland, OH, USA.

[8] Culuck, FEC., Yang, V. (1995). Overview of Combustion Instabilities in Liquid-Propellant Rocket Engines. In: Yang, V., Anderson, W. Liquid Rocket Engine Combustion Instability. Washington, DC: American Institute of Aeronautics and Astronautics, Volume 169, cap.1, p.3-37.

[9] Wooldridge., C.E., Marxman, G.A., Kier, R.J. (1970). Investigation of Combustion Instability in Hybrid Rockets. Stanford Research Institute, Final Report, NASA CR-66812, 117p.

[10] Rocker, M. (1995). Modeling of Non-acoustic Combustion Instability in Simulations of Hybrid Motor Tests, NASA/TP-2000-209905.

[11] Karabeyoglu, M.A., Zilwa, S., Cantwell, B., Zilliac, G. (2005). Modelling of Hybrid Rocket Low Frequency Instabilities. Journal of Propulsion and Power, Vol. 21, N.6.

[12] Humble, R.W., Henry, G.N., Larson, W.J. (1995). Space Propulsion Analysis and Design. 1ed. McGraw-Hill, 467p.

[13] Andrianov, A., Shynkarenko, O., Bertoldi, A. E.M., Barcelos Junior, M. N. D., Veras, C. A. G. (2015). Concept and Design of the Hybrid Test-Motor for Development of a Propulsive Decelerator of SARA Reentry Capsule. In: 51st AIAA/SAE/ASEE Joint Propulsion Conference, Orlando, USA.

[14] Bouziane, M., Betoldi A.E.M., Milova, P., Hendrick, P., Lefebvre M. (2018). Development and testing of a Lab-Scale Test-Bench for Hybrid Rocket Motors. In: SpaceOps Conference, SpaceOps Conferences, (AIAA 2018-2722), Marseille, France.

[15] Bouziane, M., De Morais Bertoldi, A. E., Lee, D., Milova, P., Hendrick, P., Lefebvre, M. (2017). Design and Experimental Evaluation of Liquid Oxidizer Injection System for Hybrid Rocket Motors. In : 7th European Conference for Aeronautics and Space Sciences (EUCASS), Milan, Italy.